



SPE 169075-MS

A methodological analysis of the mechanisms associated to steam-solvent co-injection processes using dynamic gridding

A. Perez-Perez, M. Mujica, I. Bogdanov, CHLOE, J. Hy-Billiot, Total S.A.

Copyright 2014, Society of Petroleum Engineers

This paper was prepared for presentation at the SPE Improved Oil Recovery Symposium held in Tulsa, Oklahoma, USA, 12–16 April 2014.

This paper was selected for presentation by an SPE program committee following review of information contained in an abstract submitted by the author(s). Contents of the paper have not been reviewed by the Society of Petroleum Engineers and are subject to correction by the author(s). The material does not necessarily reflect any position of the Society of Petroleum Engineers, its officers, or members. Electronic reproduction, distribution, or storage of any part of this paper without the written consent of the Society of Petroleum Engineers is prohibited. Permission to reproduce in print is restricted to an abstract of not more than 300 words; illustrations may not be copied. The abstract must contain conspicuous acknowledgment of SPE copyright.

Abstract

Hybrid steam-solvent processes have gained importance as a thermal recovery process for heavy oils in recent years. A number of pilot projects during the last decade indicates the increasing interest in this technology. Steam-solvent co-injection process aims to accelerate oil production, increase ultimate oil recovery, reduce energy and water disposal requirements and diminish the volume of emitted greenhouse gases compared to the steam-assisted gravity drainage (SAGD) process. Among the identified physical mechanisms that play a role during the hybrid steam-solvent processes are the heat transfer phenomena, the gravity drainage and viscous flow, the solvent mass transfer and the mass diffusion/dispersion phenomena. The major consequence of this complex interplay is the improvement of oil phase mobility which is controlled by the reduction in the oil phase viscosity at the edge of the steam chamber. It follows that a detailed representation of this narrow zone is necessary to capture the involved physical phenomena.

In this work, a study of sensitivity to grid size was carried out to define the appropriate grid necessary to represent the near-edge zone of the steam-solvent chamber. Our results for the steam-solvent co-injection process indicate that a decimetric scale is required to represent with a good precision the heat and mass transfer processes taking place at the edge of the steam chamber. In addition, we present some numerical results of the adaptive dynamic gridding application. Comparison was done between the SAGD process and steam-solvent co-injection after the characterization and analysis of the mechanisms which govern the oil production under the typical Athabasca oil sand conditions. Finally, in the framework of the proposed numerical methodology the effect of solvent type and injection conditions on the oil recovery efficiency is quantitatively illustrated. Published data for similar applications are also discussed.

It is expected that this work will provide some insight to the simulation community about methodological aspects to be taken into account when hybrid steam-solvent processes would be modeled.

Introduction

The steam-solvent co-injection process has recently gained popularity as an alternative process to the SAGD process. The successful pilot tests with n-butane (15 wt. %) performed at Senlac and Christina Lake are at the origin of the increasing interest in this technology. Published results show that both projects were able to increase the oil production rate by more than 30 % respect to the steam injection period (Ardali *et al.*, 2012).

In thermal processes with solvent, the main physical phenomena that control the oil productions are: gravity drainage, viscous flow, heat conduction and component mass transfer. Three first phenomena are both present in the steam-solvent co-injection and SAGD process, while the mass transfer is only important for the hybrid steam-solvent processes. The interest of the solvent-based processes is associated with the enhanced bitumen mobility at the edge of the steam chamber. The highly viscous oil moves toward the production well by gravitational force due to the viscosity reduction caused by steam-solvent condensation, conductive heat transfer and solvent solubility in the oil phase. Under the hypothesis of ideal gas behavior, the steam in presence of solvent condensates to correspondent steam partial pressure in the gas phase. Once steam condensates, the solvent mole fraction increases in the gas phase until local temperature is equal to solvent saturation temperature which causes the solvent condensation. The solvent dissolution in the oil phase is a function of pressure and temperature for a given water-solvent-bitumen system when a gas phase is present (Edmunds, 2013). Depending on solvent composition, saturation property and injection pressure, the solvent can condensate at a different temperature than steam. The additional reduction in the oil viscosity caused by the solvent dissolution in the oil phase compensates in general, the impact of the reduced temperature on the steam chamber border compared to steam only injection. It can be inferred from this that a detailed and

accurate PVT model is needed to ensure a reliable representation of solvent-bitumen behavior, the solvent solubility parameters and the oil viscosity reduction.

At the origin of the steam-solvent co-injection process, Nasr *et al.*, (2003) was one of the first who suggested that a good solvent should have a dew point close to that of steam at the injection pressure. This can favour that solvent and water condensates at the same time and maximize the oil viscosity reduction at the boundary of the steam chamber. N-hexane has relatively similar saturation temperature than steam between 25 and 35 bar. Recently, Jha and Kumar *et al.* (2013) have suggested that a lighter solvent with different saturation property than steam, like n-butane, can perform better than n-hexane at 28.5 bar. They argued that lighter solvent causes a greater reduction in the oil viscosity and reduction in residual oil saturation because of vaporization of the condensed solvent.

Concerning to the size of the liquid solvent-rich zone where molecular diffusion and dispersion occur, Sharma and Gates (2010) using an analytical model that described dynamics of thermo-solvent coupling effect in the mobile oil zone, suggested that characteristic length for catching the thermal and mass transfer phenomena at the edge of the steam-solvent chamber requires decimetric scale. Edmunds (2013) using the solution for the thermal diffusion equation applied to solvent-steam co-injection showed that a temperature gradient of 50 °C in the first meter ahead of the moving front can be expected for an average SAGD frontal velocity of 0.02 m/d. This implies that a detailed representation of the solvent-steam chamber edge is necessary in the numerical model. In order to represent appropriately this front, we propose to apply fine grid models for representing the steam-solvent condensation zone and in parallel to activate the adaptive mesh refinement option (AMR) for amalgamating the internal and external zone of the steam chamber zone. It is expected that with this simulation strategy a detailed representation of the front will be caught by a fine model while a coarse model will be enough to represent the heat transfer phenomenon that dominates in the non-critical zone.

In this work, we perform steam-solvent co-injection simulations in a 2-D synthetic reservoir model using the dynamic grid amalgamation process present in STARS (CMG) commercial reservoir simulator. Firstly, we compare results obtained in a fine model applied to steam-solvent co-injection process vs. some results obtained using the AMR with different parameters. The main purpose of this task is to identify some parameters that properly trigger the amalgamation process during a steam-solvent injection process. Later, we evaluate the gridblock size effects on the steam-solvent co-injection process using the amalgamation procedure with the parameters defined in the previous step. With the purpose of elucidating which solvent performs better under different conditions, we show results after injecting different solvents. We evaluate the effect of solvent type and injection pressure during the steam-solvent co-injection process with pure n-hexane, pure n-butane and a mixture of n-hexane-n-butane 50 v./v. co-injected with steam at 25 and 35 bar. A steam injection case was run as a base line case. The purpose is to compare its performance and to explain differences in obtained results. Comparisons are performed based on temperature, saturations, solvent concentration, oil viscosity and mobility profiles and productivity indicators.

This work is innovative in the sense that it proposes the use of dynamic gridding in a fine model to follow in details the steam-solvent front. In addition, we have included solution gas (CH₄) in the model. According to the authors, these features applied to steam-solvent co-injection process have not been previously published in the literature.

Amalgamation process

Here we describe briefly the process developed by Sammon (2003) about amalgamation. The amalgamation process consists in creating an object (a group of fine cells) when gradients of identified properties in the amalgamation domain are smaller than threshold values defined by the user. If the gradient of a specified property is larger than the defined thresholds in the domain, calculation proceeds with fine grid blocks. When the simulator should assess the amalgamation state, it generates temporarily the finest scale grid possible. The simulator populates this grid by passing all properties values from any previously existing coarse objects to the child cells (porosity permeabilities, saturations). Then gradients for all properties are calculated. Each possible coarse object is considered in turn for creation. An object (the amalgamated cell) is created if sufficiently small differences exist between the neighboring fine scale of the potential coarse object and their fine scale neighbors within the object. A control list specifies the properties and the level of change to be screened before deciding if some cells will be amalgamated or de-amalgamated. The control list includes temperature, saturation, composition per phase and global composition. Once the simulator has decided where conditional refinements and amalgamation can be done, the primary simulator properties are up-scaled. Most of up-scaling is by pore-volume weighted averaging and by direct summation for mass-based quantities. Intercell connections for amalgamations are built up from the list of finest-scale connectivities. Once upscaling and connection building processes are complete, the simulator computes the new resulting grid.

The dynamic gridding features have been fully integrated with the adaptive implicit formulation used in the thermal simulator (STARS) and with their dispersion and diffusion modeling capabilities. Some validation tests have been published in the literature for different EOR processes (Sammon, 2003; Darche *et al.*, 2004).

For all simulations in this work, initial grid begins with fine gridblocks. Once run progresses, the dynamic gridding procedure is applied. The zones with important property changes keep fine gridblocks while zones with small property gradients are amalgamated in blocks of 1x1m. Figure 1 shows temperature and solvent molar fraction in oil phase when steam-n-butane is co-injected in a SAGD pair. In this case two properties are specified to trigger the dynamic gridding at the front. As larger temperature and oil molar fraction changes occur at the edge of the steam chamber due to the steam-solvent

condensation, a fine model is kept to catch principal phenomena in this region while a coarse model is automatically generated abroad.

Model description

In the following sub-section, the reservoir model and operational conditions are described.

Synthetic reservoir model

A synthetic reservoir representing a generic formation of Athabasca oil sands (western Canada) is used in this work. The reservoir consists of a pay zone rich in oil. The pay zone is 45.5 m in length (x direction) and 50 m in thickness (z direction).

For simulating the SAGD recovery process, a horizontal production well (P) with a length of 850 m (y direction) is placed 1.5 m above the bottom of the pay zone. A horizontal injection well (I1) with the same length is situated parallel to the producer well with a 5 m vertical well spacing. The horizontal spacing between well pairs is around 91 m. Due to symmetry and the assumption of a homogeneous system; we model only half of the unit. A non-uniform 2-D Cartesian grid system is used in the simulation. This grid contains 5 grid blocks in the x-direction of 0.1 m and then 90 gridblocks of 0.5 m. The number of grid blocks in the z-direction is 50. A fraction equals to 0.5 is specified for both wells in order to adjust its corresponding well indexes to the half representation of the reservoir.

Initial oil and water saturation in the pay zone are 0.8 and 0.2, respectively. Initial reservoir temperature is 10°C. The reservoir formation consists of clean sand. The absolute permeability in the pay zone is 2 Darcy in the horizontal direction while vertical permeability is 3/5 of the horizontal permeability. Porosity is 35%. Heat losses from and to over burden and under burden are specified. Some reservoir properties and relative permeability end-points are listed in Table 1. A live oil fluid model is used in our simulation. Water, heavy oil, methane and solvents (n-hexane and/or n-butane) are specified in the numerical model. Molar fraction of methane dissolved in oil is 0.037 at reservoir conditions. Phase partition coefficients for the k-value function were taken from the literature (STARS manual) for the solvents. Heavy oil viscosity is 8028 cP at 50°C. A decreased function of oil viscosity as a function of temperature was used for a heavy Athabasca oil. Solvent pseudo-viscosities were taken from Ardali, Mamora and Barrufet (2010). Oil phase viscosity was obtained by the natural logarithmic mixing rule currently used in the simulator. Bitumen viscosity and solvents pseudo-viscosities are shown in Table 2 for three temperatures. Values at 150 °C are interpolated from an adjusted power-law function for the solvents. Gas viscosity of hydrocarbon components is fixed at 1E-02 cP. No solvent dependency effect in the relative permeability end-points was considered in our simulations. Diffusion and dispersion coefficients were not specified in these simulations because there is not enough data in the literature related to the scaled solvent-dispersion coefficients. Asphaltene precipitation model and water dissolution in oil phase were neither considered in this model. It is expected that the current model simplification permits to understand the main phenomena that occur during the steam-solvent co-injection process without specifying explicitly dispersive processes. Once complex phenomena are well understood, more complexity could be added to this model.

Operational conditions

The steam injector is controlled in pressure and in steam injection rate. The injector well is operated at a maximum bottom-hole pressure of 25 (or 35 bar) and maximum water injection of 450 m³/d for the SAGD pair studied in this work. The steam quality is 90%. A pre-heating period of three months is performed before the steam injector is open. The steam-solvent co-injection process is analyzed for only five years to minimize the border effect in the numerical results. The operational strategy followed in this study is as follows unless stated differently: one year of steam injection, followed by one year of steam-solvent co-injection and three additional years of steam. Maximum water injection is not explicitly reduced during the co-injection period. Solvent-steam volume ratio is 0.20 volume fraction unless otherwise noted.

Steam-solvent co-injection process in a fine model vs. fine model with dynamic gridding

The main purpose of this activity is to select the appropriate parameters that can give similar results to those obtained from a fine model when a hybrid steam-solvent process is run. A steam-n-hexane co-injection model is built for this particular purpose in order to compare results obtained from a fine model with an elemental gridblock of 0.1x0.1m and from the same fine model running with the dynamic gridding option. A period of one year of steam-solvent co-injection was studied in this section due to high calculation time for the fine model. The amalgamated zones are defined as 1x1m, so a set of fine cells can be lumped into a big one ten folds larger. The resulted coarse cell has a surface one-hundred folds higher than the elemental fine gridblock. The amalgamation process occurs when calculated property gradients are smaller than property gradients specified in the model. If changes in the selected properties exceed the defined threshold, a fine gridding is kept for those cells.

For running the adaptive mesh refinement procedure, a sensitive analysis is performed for three selected properties that were evaluated as appropriate to follow the steam-solvent front. These properties are: temperature, oil phase mole fraction and gas phase mole fraction. In general, temperature and oil mole fraction changes define the location where steam and solvent begin to condensate. The gradient in gas mole fraction is also selected to indicate the point where condensable components change from the gas phase to the liquid phase. The maximum gradients in temperature, oil molar fraction and gas molar fraction are defined as 10°C, and 0.05 and 0.05, respectively. A number of five timesteps is defined as the minimum interval to

perform checks to evaluate changes due to dynamic amalgamation. The following four cases are tested to evaluate the effect of the trigger properties and selected gradients in a fine steam-solvent co-injection model:

- Three properties
 - TEMPER (10) and OMOFRC(0.05) and GMOFRC(0.05)
- Two properties
 - TEMPER(10) and OMOFRC(0.05)
- Only one property
 - TEMPER(10) or OMOFRC(0.05)

Figure 2 to Figure 5 show some horizontal profiles in a selected reference line (8 m from reservoir bottom) for the studied cases. All cases injected steam and solvent for one year using a fine model (0.1x0.1m). Injected solvent is n-hexane while solvent-steam volume ratio is 0.10 volume fraction. A reference case was solved in a fine model without dynamic gridding. Abscissa-scale is cut (15 m) to appreciate more in detail the horizontal profiles. At the reference line, pressure is constant and temperature is equal to saturation temperature at steam partial pressure in the gas mixture. At the center of the steam chamber, solvent presence in gas phase is relatively low to alter significantly steam chamber temperature. This results in local temperature close to steam saturation temperature ($T_{\text{sat}} \approx 224^\circ\text{C}$ at 25 bar absolute (NIST, 2014)). At the steam chamber edge (8 m from steam chamber center), steam begins to condensate when local temperature equals to correspondent temperature of steam partial pressure. Solvent also condensates because its saturation temperature is close to that of steam at injection pressure ($T_{\text{sat}} \approx 221^\circ\text{C}$ at 25 bar absolute (NIST, 2014)). Water and oil saturation increase due to simultaneous water and solvent condensation. Condensed solvent is counted in oil saturation. The increment in solvent mole fraction in oil phase creates a liquid solvent-rich zone. According to Figure 3 and Figure 4, the liquid-solvent rich zone thickness is around four meters after one-year steam-solvent co-injection. This high solvent concentration reduces significantly oil viscosity which consequently improves oil mobility (Figure 5). Figure 3 to Figure 5 show a relative large dispersion and a right shift in saturations, oil molar fractions, oil viscosity and oil mobility when only one property (TEMPER or OMOFRC) is used to control the amalgamation process. This suggests a clear deviation with respect to the fine model (marked as a reference model in the figures). A priori using two or more properties to control the dynamic gridding process gives similar results. However, calculation time is significantly different when multiple properties are used to control the amalgamation process. Figure 6 compares calculation time for the four cases studied. Calculation time for the fine model was 106 h. According to this figure, the use of three properties spends around twice as much time than with two parameters. These figures suggest that the use of dynamic gridding with two parameters can generate a speed-up of around 15 folds when comparing with a fine model. Profile results and calculation time show that dynamic gridding with two parameters is appropriate to mimic results obtained with a fine model applied to steam-solvent co-injection process. This demonstrates that dynamic gridding can be successfully employed for simulation models that need to perform calculation in a relatively fine model.

Figure 7 shows how condensed solvent in oil phase expands as a function of time during one year of steam-solvent co-injection in a fine model without dynamic gridding. Solvent-rich zone enlarges with time because global solvent concentration increases in the system during the injection process. Liquid-solvent rich zone reaches laterally 1 m after 3 months, 1.5 m after 6 months and around 4 meters at the end of the first year of steam-solvent co-injection. This zone is relatively thinner on the steam chamber top with sizes lower than 1 meter after 1 year of injection. These results suggest that the selection of a decimetric scale to model the liquid-solvent rich zone is necessary to catch physical phenomena that occur at the steam-solvent chamber edge.

The identification of properties and definition of thresholds that define the water-oil interface using dynamic gridding were performed for three steam-solvent co-injection cases: n-hexane-steam, n-butane-steam and propane/n-butane/n-hexane-steam. The use of property gradients that trigger the amalgamation option (TEMPER=10°C and OMOFRC=0.05) for the whole solvents evaluated resulted in good consistency with those obtained from the fine model. The use of smaller property gradients (TEMPER=5°C and OMOFRC=0.05) was also tested with similar results but slightly larger calculation time. It is expected that this simple parameterization will be valid for other solvents under different operational conditions. However, it can be convenient to evaluate more complex co-injection cases (i.e. naphtha or a lumped solvent) and to validate that results are consistent with those obtained on the fine model.

Effect of gridblock size

Once parameters that control the amalgamation process have been defined, we proceed to figure out the minimum size needed for modeling the steam-solvent injection process at field scale. The main objective of this part is to define the elemental gridblock size that permits to catch the steam-solvent liquid zone. We evaluate the following elemental gridblock sizes:

- 0.2x0.2 m
- 0.5x0.5 m
- 1x1 m
- 2x1 m

A steam-solvent co-injection process was run for five years, starting with one year of steam injection and followed by one year of steam-solvent co-injection and then, three years of steam injection. Results for very small gridblocks (0.1x0.1m) are not shown here due to large calculation time. Relative large gridblocks (2x1) were selected to show the effect of the coarse representation in a field model. Figure 8 shows results for cumulative bitumen production. Considering that calculation time for 0.5x0.5m case was 18 folds faster than that of 0.2x0.2m case, we conclude that performing simulations with Cartesian gridblock sizes of half-meter is adequate to obtain a good resolution of the phenomena occurring at the front edge.

These results do not take into account the mass dispersion phenomena. We tested the effect of including some n-hexane dispersion coefficients proposed by Deng, Huang *et al.* (2010). We use values for solvent dispersion coefficients in oil and gas phase of $1.4\text{E-}05 \text{ m}^2/\text{d}$ and $7.2\text{E-}04 \text{ m}^2/\text{d}$, respectively in our numerical simulations. These values were obtained from a history match process applied to steam-solvent experiments. These solvent dispersion coefficients were not up-scales. We did not observe changes in the results for the gridblock sizes evaluated in this work. Some authors (Deng, Huang *et al.*, 2010; Singh and Babadagli, 2011) have suggested that steam-solvent co-injection process is controlled by thermal diffusion and gravity-dominated processes and solvent diffusion has a minor effect on results.

Effect of solvent type

Three different solvents are evaluated to compare their performance and to explain the differences during the steam-solvent co-injection process: pure n-hexane, pure n-butane and a mixture 50 vol. % n-hexane and 50 vol. % n-butane. All studied cases injected 20% volume of solvent per volume of total fluid injected; all in liquid phase. Table 3 shows volume fractions and correspondent mole fractions of water and solvents injected. Dynamic gridding was employed in these runs in order to amalgamate 0.5x0.5m gridblocks in the region abroad of the front to 1x1 m. Injection pressure is 25 bar. A SAGD case was run as a reference case for comparison purpose.

Figure 9 to Figure 12 show steam and steam-n-hexane co-injection profiles taken at 20 m from reservoir bottom. Profiles are shown after injecting steam for one year and steam-solvent for six months. Abscissa scale is cut to appreciate more in detail the profiles. Left side represents the middle of the steam chamber while right side represents the untouched reservoir zones by steam and/or solvent. Due to solvent presence in the steam chamber for the steam-solvent co-injection case, steam partial pressure (P_{water}) reduces proportionally to total pressure (P) and steam mole fraction in the gas phase ($y_{\text{water}}=1-y_{\text{methane}}-y_{\text{solvent}}$). Once the temperature has reduced to approximately $T=T_{\text{sat}}(P_{\text{water}})$, water condensation occurs. As previously discussed, because of relatively similar saturation temperature for water and n-hexane at 25 bar, local temperature reaches $T=T_{\text{sat}}(P_{\text{n-hexane}})$ and solvent condensation arises. Figure 10 and Figure 11 show that water saturation and solvent mole fraction in gas/oil phase increase at around 5 m. At this point gas saturation reduces, water saturation and solvent mole fraction in oil phase increase. These simultaneous increments show that water and n-hexane condensate at the same point. Reduction in local temperature is now more evident than for the steam injection case due to relatively high solvent concentration in the gas phase. The increment in dissolved solvent in oil causes an increment in oil saturation. A non-zero gas saturation zone can be observed in the gas phase between 6.5 and 8.5 m. This is due to methane presence. Methane is generally situated at the colder region (right side) of the steam chamber. This methane rich zone creates later a path to reach the producer well. Maximum solvent concentration in gas and oil phase occurs at 0.5 m apart. Maximum solvent mole fraction in oil phase occurs at 7.5 m and it defines the point of minimum oil viscosity. At this point, oil mobility finds consequently its maximum. A reduction in oil viscosity of one order of magnitude has been observed when comparing results from steam-n-hexane and steam injection case. The 3.5m-thick solvent-rich zone after six months of steam-solvent co-injection highlights the importance to use fine gridblocks at the steam chamber edge. Towards the steam chamber edge, thermal diffusion controls the process and the resulting local temperature tends to equalize when steam case and steam-n-hexane case are compared (*cf.* Figure 9).

Figure 13 to Figure 15 show respectively temperature, oil viscosity and oil mobility horizontal profiles for steam and the different solvents studied in this work. Due to high n-butane volume fraction injected (*cf.* Table 3), condensation temperature is sensibly affected when steam-n-butane and steam-mixture are co-injected. The high solvent mole fraction in gas phase causes that steam condensates sooner for steam-n-butane case than for steam-n-hexane case. Once the temperature has reduced to approximately $T=T_{\text{sat}}(P \cdot y_{\text{water}})$, water condensation occurs, leaving more butane in the gas phase. As phase partition coefficient of n-butane becomes smaller at low temperature ($k=y_i/x_i$) n-butane in the oil phase increases. High local solvent concentration in oil causes a minimum in oil viscosity. This occurs two or three meters away from steam condensation point. N-hexane co-injection case produces the lowest oil viscosity even if solvent viscosity for n-butane is lower than for n-hexane at any temperature (*cf.* Table 2). Oil viscosity differences (from 1 to 3 cP at reservoir conditions) are minimal at this point; however this affects notably the oil phase mobility. In consequence, n-hexane co-injection case results in higher mobility than n-butane or n-butane/n-hexane mixture cases. This fact highlights the importance of having an accurate oil viscosity model at high temperature for bitumen and solvents built on PVT measurements.

The effect of solvent type in some productivity indexes: bitumen recovery, solvent recovery and steam-to-oil ratio is discussed now. Figure 16 shows bitumen recovery after 5 years of hybrid steam-solvent co-injection. Solvent production was subtracted from calculation to have only bitumen production. N-hexane gives better recovery due to larger oil mobility at the front. N-hexane co-injection produces around 1.5% more bitumen in volume basis than n-butane and n-butane/n-hexane mixture cases. Different types of solvents have been studied in the literature via numerical simulations (Ardali, Mamora and Barrufet, 2010; Li and Mamora *et al.*, 2011; Yazdani *et al.*, 2012; Ardali *et al.*, 2012). Results indicates that heavier solvents

(n-hexane or higher) are preferable for injection pressures between 15 and 25 bars while lighter solvents (e.g., n-butane) is suitable for injection pressures between 35 and 40 bars. Some of these authors signaled that results are strongly dependent of fluid characterization (PVT data), and operational conditions. We confirm that solvent selection requires a detailed phase behavior description and accurate fluid dynamic in order to precisely which solvent performs better under particular conditions.

Figure 17 shows solvent recovery in mole fraction produced by mole of solvent injected for the selected solvents. The major solvent recovery results for n-hexane which has a larger mole fraction in the oil phase with respect to the total number of mole injected. It is worth noting that solvent production tends to stabilize at the end of co-injection period (2 years). Solvent recovery reaches only 20-40 % mole produced by mole injected at the same time period. Then solvent production re-accelerates for one-year more when only steam is injected. Solvent recovery slows down after that time. Figure 18 shows cumulative steam-to-oil ratio (CSOR) for steam injection and selected solvents. As expected, an important reduction in the CSOR occurs at the beginning of steam-solvent co-injection period due to oil production up-lift and less injected steam in the reservoir. Steam-solvent injection cases have a CSOR of around one unit lower than this of the steam injection case once solvent is co-injected.

Effect of injection pressure

The effect of injection pressure was tested for different fluids. Injection pressure was fixed at 35 bars during a five-year injection period. The fact to inject saturated steam at higher pressure implies higher saturation temperature ($T_{\text{sat}} \approx 243^\circ\text{C}$ at 35 bar vs. 224°C at 25 bar for pure water). Figure 19 shows oil mobility profiles at the same reference point considered in the previous cases (Figure 15). These profiles are extracted after one year of steam injection and 0.5 year of steam-solvent co-injection. Oil mobility profiles are surprisingly high for all solvents when steam-solvent are co-injected at high pressure. This uniform high oil mobility results in a better bitumen recovery factor for n-butane and n-butane/n-hexane cases respect to values obtained at low pressure. Figure 20 shows bitumen recovery factors for different solvent injected at 35 bar. When n-butane is injected at high pressure, oil recovery is similar to that obtained for n-hexane. This confirms that n-butane performs better at high injection pressure (35 bar) than at low pressure (25 bar).

Final comments

The validity of results presented in this work is conditioned to simulation inputs, in particular PVT model: fluid phase behavior and viscosity model. However, the methodology described here can be applied to any hybrid steam-solvent process based on reliable experimental data and on accurate PVT modeling. This methodology provides enough precision to take into account major physical phenomena that occurs at the steam-oil interface. The use of this methodology can be also employed in thermal processes based on reactive systems like, in situ combustion (ISC), in situ upgrading (ISU) where the use of fine-scale mechanistic models are needed.

The use of coarse models causes a reduction in the maximum of solvent concentration in the oil phase which affects directly the front displacement. The calculated local temperature in a coarse model also affects the location where steam and solvent condensate due to non-enough discretized temperature and pressure. This results in a rough front representation which derives in a less efficient thermal recovery process.

It is expected that the current methodology applied to steam-solvent co-injection process will be tested using dynamic gridding in a heterogeneous reservoir. The main objective is to identify in which cases amalgamation function can properly work in a heterogeneous porous media. Preliminary non-published results performed by the authors in a heterogeneous reservoir suggests that front shape is not identical at any time and a delay in the front displacement can occur when comparing results obtained from a fine model and those obtained from a model after applying dynamic gridding. Additional effort should be done to understand how the amalgamation process, forward and behind of the moving front, can alter the front movement and how solvent dispersion can counteract this effect.

Conclusions

- Dynamic gridding can be successfully employed for simulation models that need to perform local calculations in a fine model with a reduction in computation time.
- Selection of a decimetric scale to model the liquid-solvent rich zone is necessary to catch main physical phenomena that occur at the steam-solvent chamber edge. These phenomena are: steam-solvent condensation, solvent dissolution, oil viscosity reduction and gravity segregation.
- The property gradients and thresholds that control the amalgamation process were identified when gridblocks were lumped 10 folds in each direction in a fine model (0.1x0.1m). Results obtained with two-property gradients (temperature=10 & oil molar fraction=0.05) are in good consistency with results obtained on the fine model. A speed-up of around 15 folds was obtained when comparing calculation time using the fine model and the fine model with dynamic gridding.
- Maximum solvent concentration in oil phase defines a region of maximum oil mobility in the steam chamber edge. Injection pressure and solvent type play an important role in the location and intensity of the oil mobility peak.

- N-butane could be envisaged as a prospective solvent when injection pressure is around 35 bar. However, n-hexane performs well at both pressures: 25 and 35 bars. Both results are limited to the validity of thermodynamic data employed in this work.

Acknowledgements

TOTAL S.A. is gratefully acknowledged for sponsoring this research work. Computer Modelling Group (CMG) is acknowledged for the permission to use STARS reservoir simulator.

References

- Ardali, M., Barrufet, M.A., Mamora, D. (2012, October 8-10) "A critical review of hybrid steam-solvent processes to recover heavy oil", SPE paper 159267, paper presented at the SPE annual technical conference in San Antonio, Texas.
- Ardali, M., Mamora, D. D., & Barrufet, M. (2010, January 1). "A Comparative Simulation Study of Addition of Solvents to Steam in SAGD Process". Society of Petroleum Engineers. doi:10.2118/138170-MS
- Ardali, M., Mamora, D., & Barrufet, M. A. (2011, January 1). Experimental Study of Co-injection of Potential Solvents with Steam to Enhance SAGD Process. Society of Petroleum Engineers. doi:10.2118/144598-MS
- Darche, G., Grabenstetter, J. E., & Sammon, P. H. (2005, January 1) "The Use of Parallel Processing with Dynamic Gridding". Society of Petroleum Engineers. doi:10.2118/93023-MS.
- Deng, X., Huang, H., Zhao, L., Law, D. H.-S., & Nasr, T. N. (2010, January 1) "Simulating the ES-SAGD Process With Solvent Mixture in Athabasca Reservoirs". Society of Petroleum Engineers. doi:10.2118/132488-PA.
- Edmunds, N. R. (2013, June 11) "Observations on the Mechanisms of Solvent-Additive SAGD Processes". Society of Petroleum Engineers. doi:10.2118/165419-MS.
- Jha, R., Kumar, M., Benson, I., & Hanzlik, E. (2013, July 1) "New Insights into Steam/Solvent-Coinjection-Process Mechanism". Society of Petroleum Engineers. doi:10.2118/159277-PA.
- Li, W., Mamora, D. D., & Li, Y. (2011, June 1). "Solvent-Type and -Ratio Impacts on Solvent-Aided SAGD Process". Society of Petroleum Engineers. doi:10.2118/130802-PA.
- Nasr, T. N., Beaulieu, G., Golbeck, H., & Heck, G. (2013, January 1) "Novel Expanding Solvent-SAGD Process "ES-SAGD."". Petroleum Society of Canada. doi:10.2118/03-01-TN.
- NIST Standard Reference Database 69: NIST Chemistry WebBook (2014, February 06). NIST Reference Fluid Thermodynamic and Transport Properties Database. Web site: <http://webbook.nist.gov/chemistry/fluid/>
- Sammon, P. H. (2003, January 1) "Dynamic Grid Refinement and Amalgamation for Compositional Simulation". Society of Petroleum Engineers.
- Sharma, J., & Gates, I. D. (2010, January 1) "Dynamics of Steam-Solvent Coupling at the Edge of an ES-SAGD Chamber". Society of Petroleum Engineers. doi:10.2118/128045-MS.
- Singh, R., & Babadagli, T. (2011, January 1). Mechanics and Upscaling of Heavy Oil Bitumen Recovery by Steam-Over-Solvent Injection in Fractured Reservoirs Method. Society of Petroleum Engineers. doi:10.2118/132459-PA
- Yazdani, A., Alvestad, J., Kjoensvik, D., Gilje, E., & Kowalewski, E. (2012, July 1). "A Parametric Simulation Study for Solvent-Coinjection Process in Bitumen Deposits". Society of Petroleum Engineers. doi:10.2118/148804-PA

Table 1. Reservoir properties and dynamic parameters.

<i>Properties</i>	
Reservoir depth (top of pay zone)	270 m
Initial reservoir pressure at 270 m	1150 kPa
Thickness	50 m
Porosity	0.35
Horizontal permeability	2000 mD
Vertical permeability	1200 mD
Oil viscosity at 50°C	8028 cP
Initial temperature	10°C
Initial oil saturation	0.8
Methane molar fraction in oil at RC	0.037
Initial water saturation	0.2
Oil gravity	8 API
Connate gas saturation, Swc	0.07
Residual liquid saturation to gas, Slrg	0.26
Residual oil saturation to gas, Sorg	0.19
Critical gas saturation, Sgc	0.10

Table 2. Pseudo-viscosities for some components at three temperatures

<i>Pseudo-liquid viscosity, cP</i>	<i>20°C</i>	<i>150°C</i>	<i>220°C</i>
Bitumen	319000	30.92	7.01
n-butane	20.0	1.54	0.51
n-hexane	36.4	2.53	0.66

Table 3. Injected water-solvent volumes/mole fractions in the studied cases

<i>Injection at 15 °C and 101.3 kPa</i>	<i>Hexane case</i>	<i>Butane case</i>	<i>Mixture case</i>
Volume fraction injected			
Water	0.7999	0.0164	0.0322
n-butane	-	0.9836	0.9638
n-hexane	0.2001	-	0.0040
Molar fraction injected			
Water	0.9668	0.9563	0.9615
n-butane	-	0.0437	0.0220
n-hexane	0.0332	-	0.0165

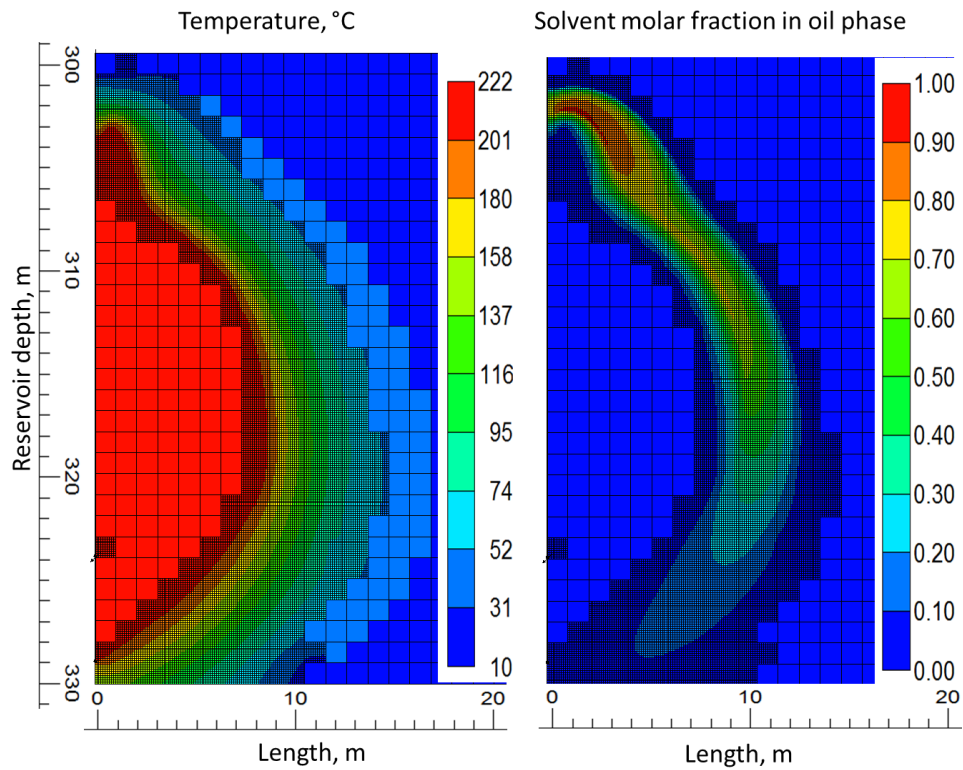


Figure 1. Temperature and solvent molar fraction in oil phase with dynamic gridding at the front.

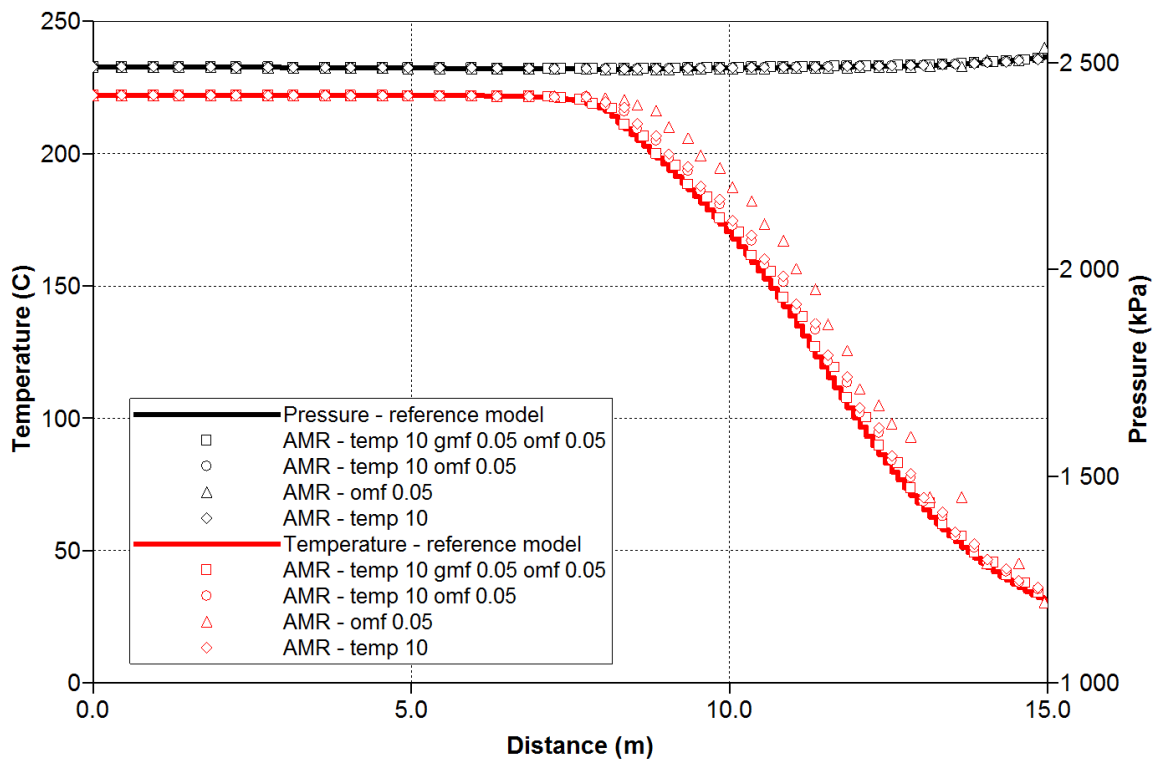


Figure 2. Temperature and pressure horizontal profiles for a fine steam-solvent co-injection model with different levels of activity in some control properties of dynamic gridding.

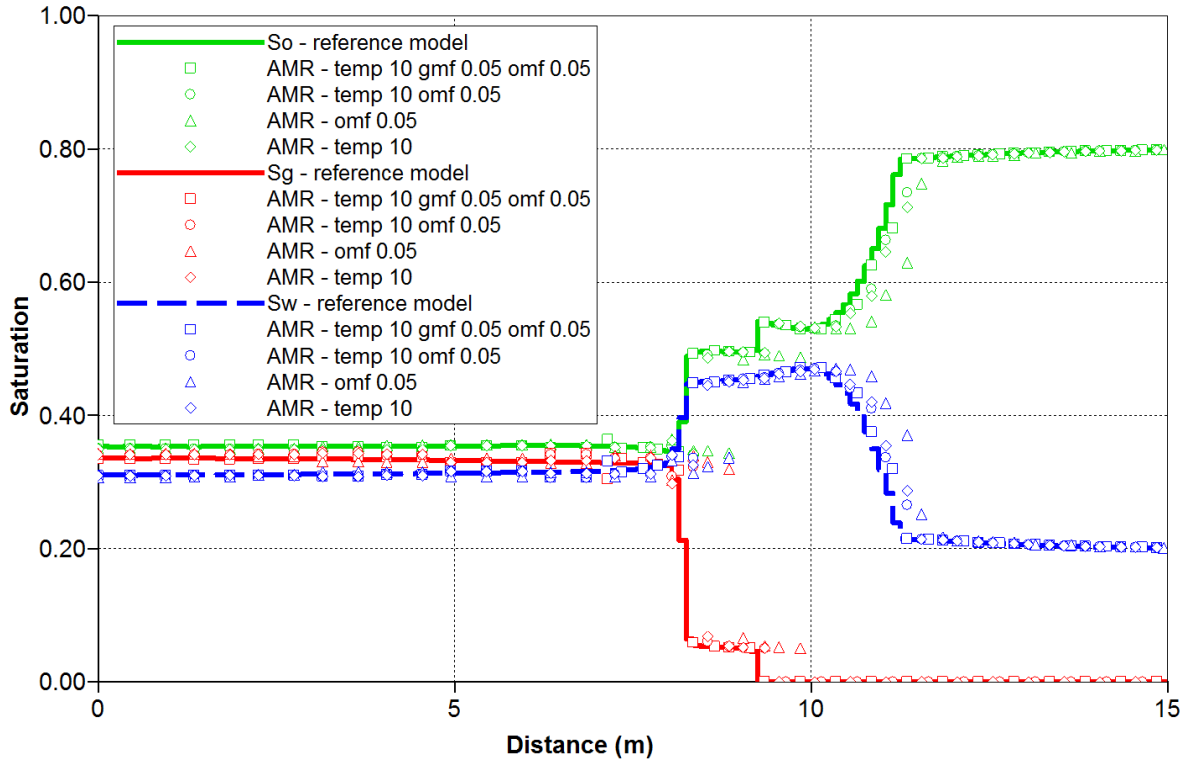


Figure 3. Saturation horizontal profiles for a fine steam-solvent co-injection model with different levels of activity in some control properties of dynamic gridding.

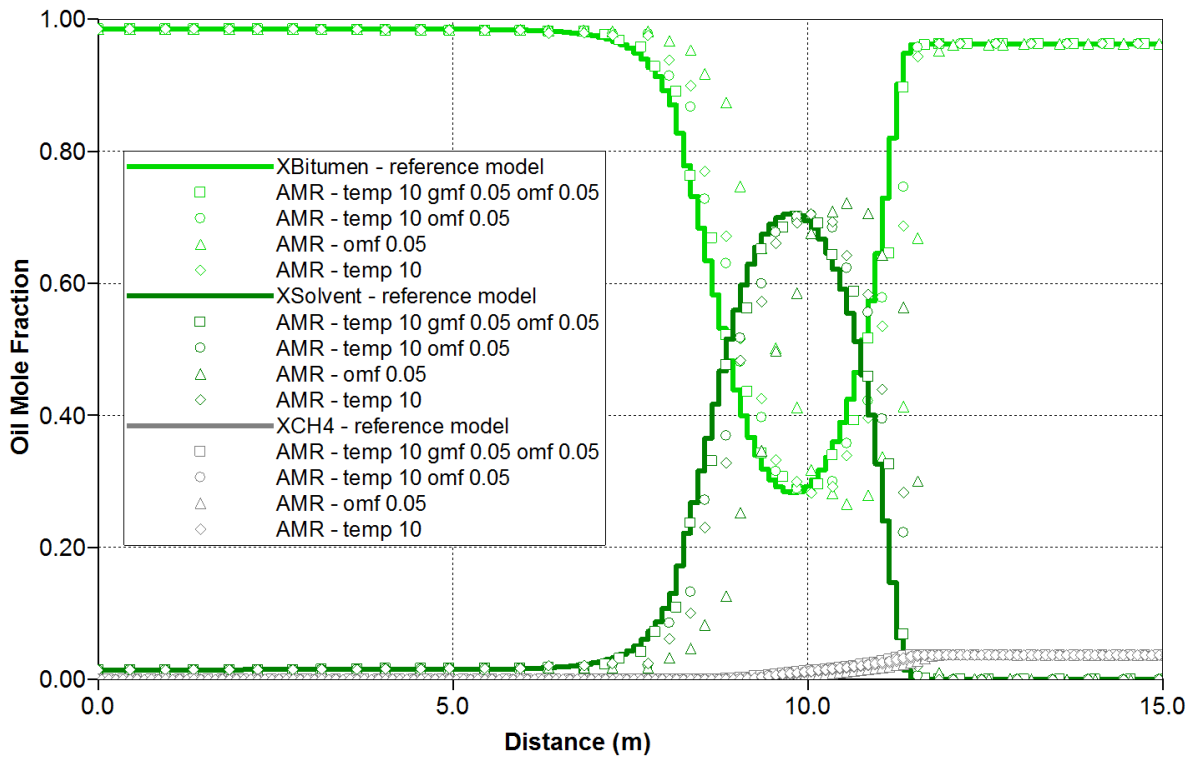


Figure 4. Oil mole fraction horizontal profiles for a fine steam-solvent co-injection model with different levels of activity in some control properties of dynamic gridding.

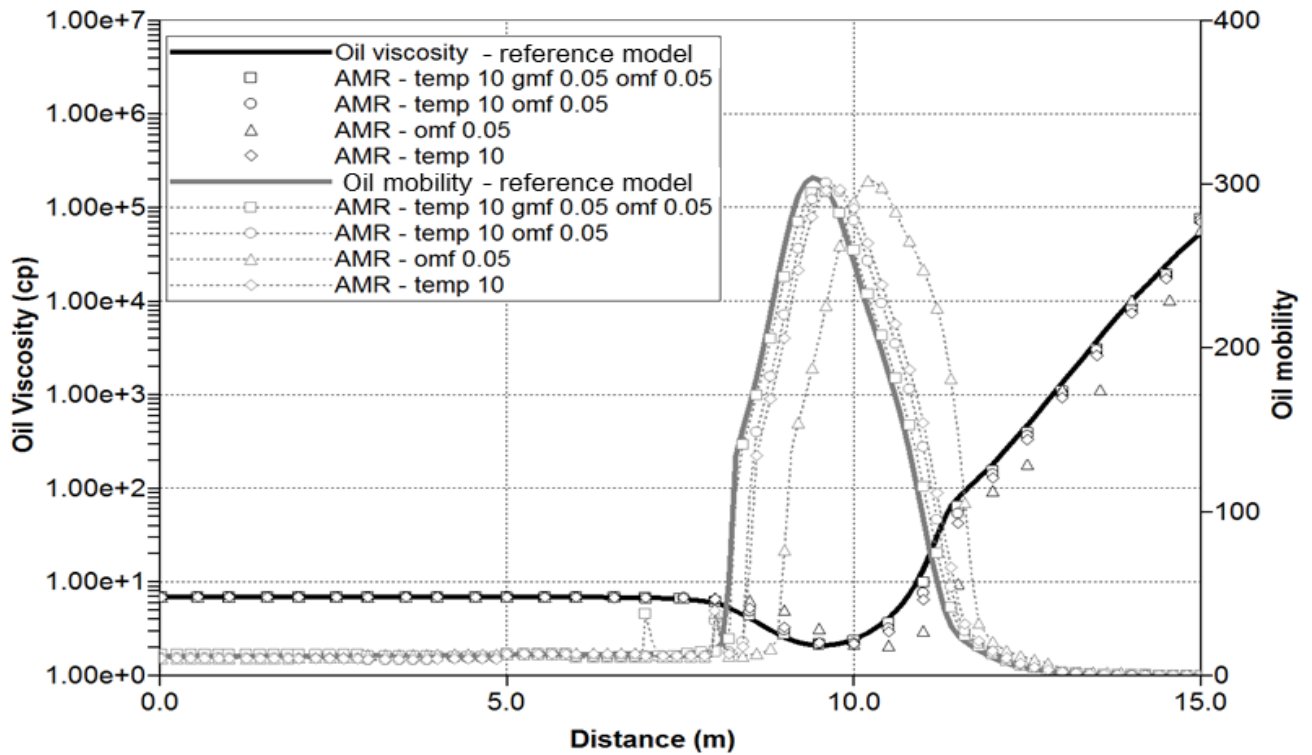


Figure 5. Oil viscosity and oil mobility horizontal profiles for a fine steam-solvent co-injection model with different levels of activity in some control properties of dynamic gridding.

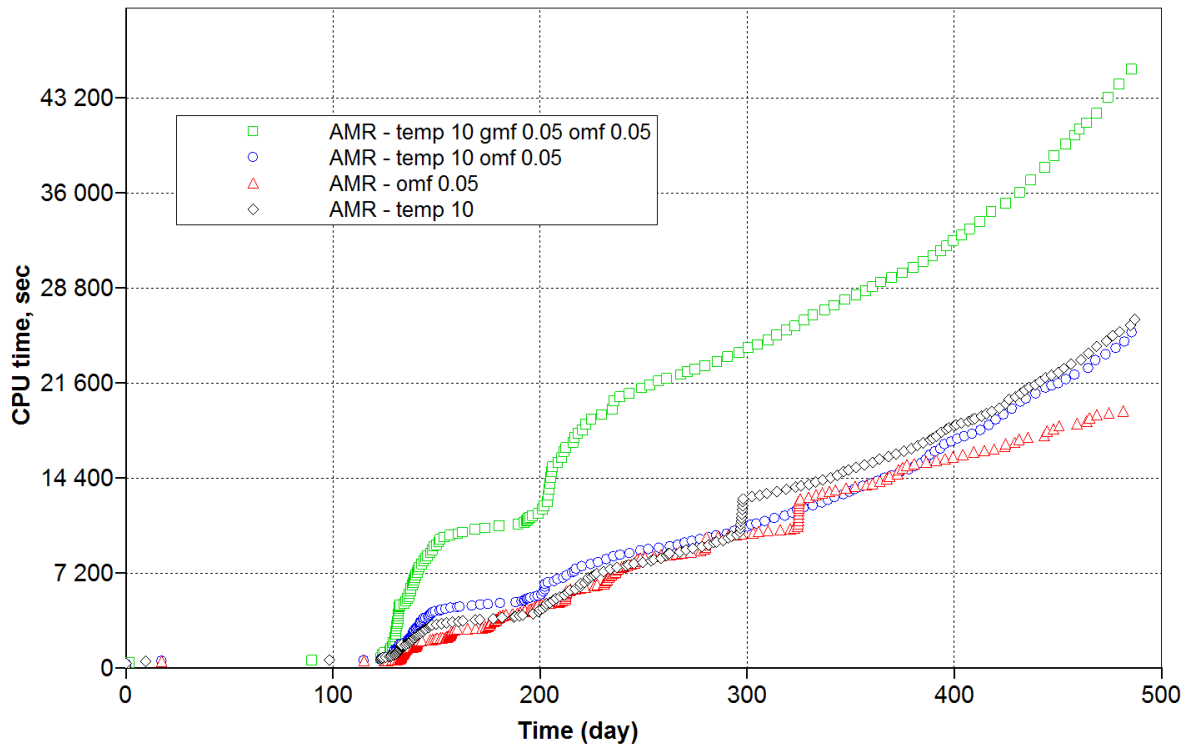


Figure 6. Calculation time for the different studied cases with dynamic gridding.

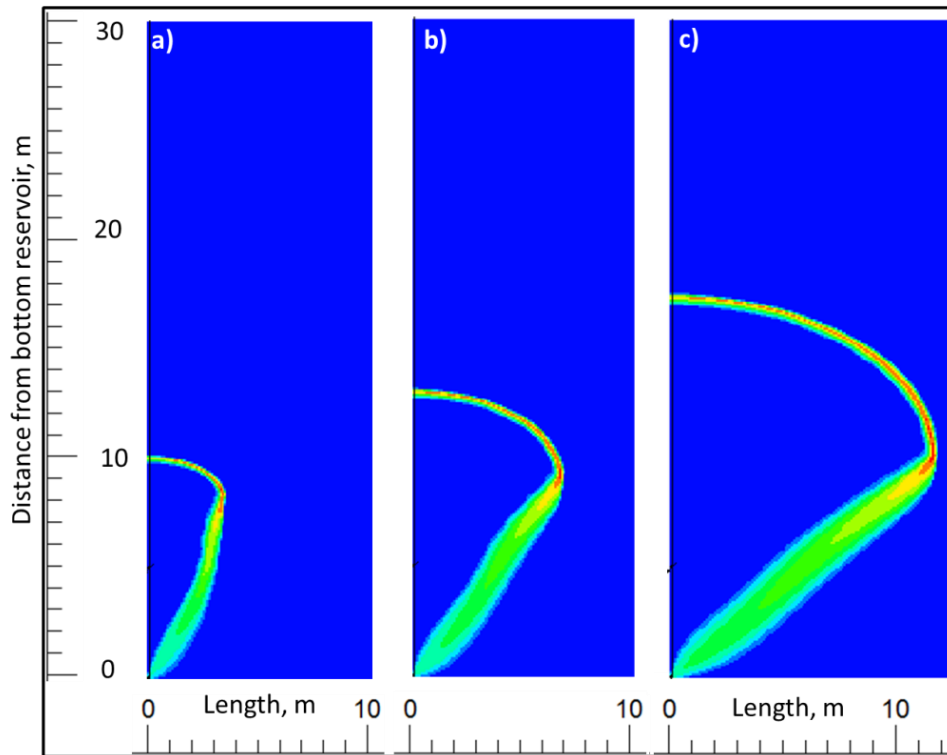


Figure 7. Solvent mole fraction in oil phase for) 3 months b) 6 months c) 12 months of steam-solvent co-injection for a fine model.

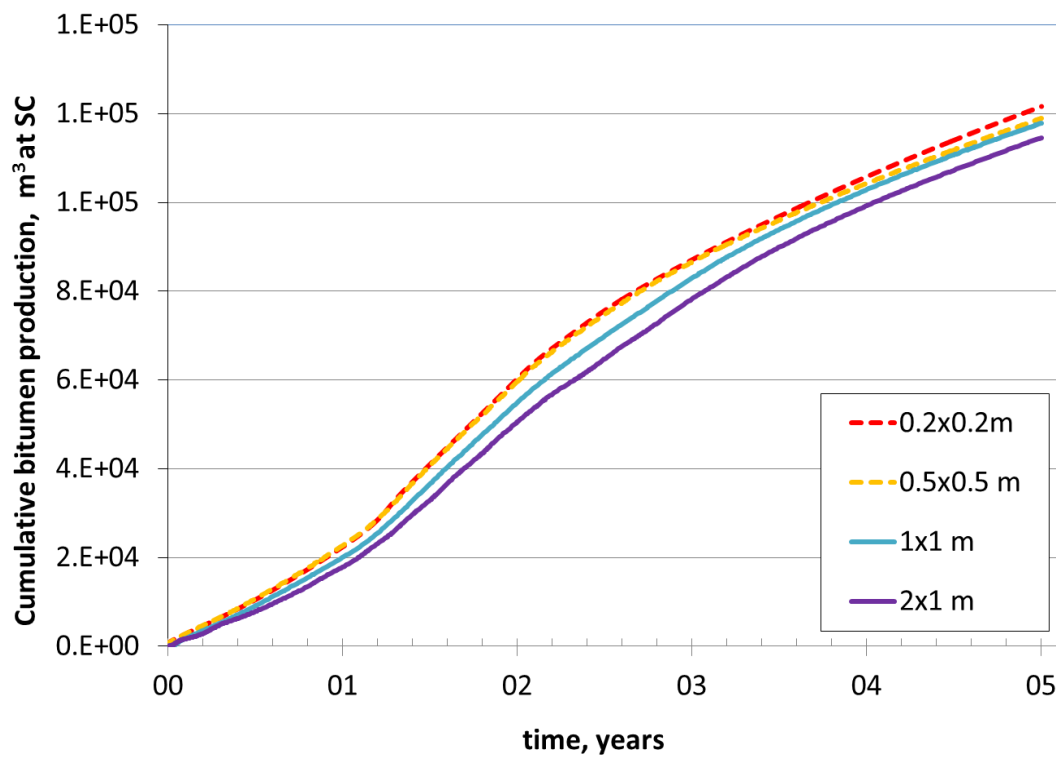


Figure 8. Cumulative bitumen production for different gridblock sizes.

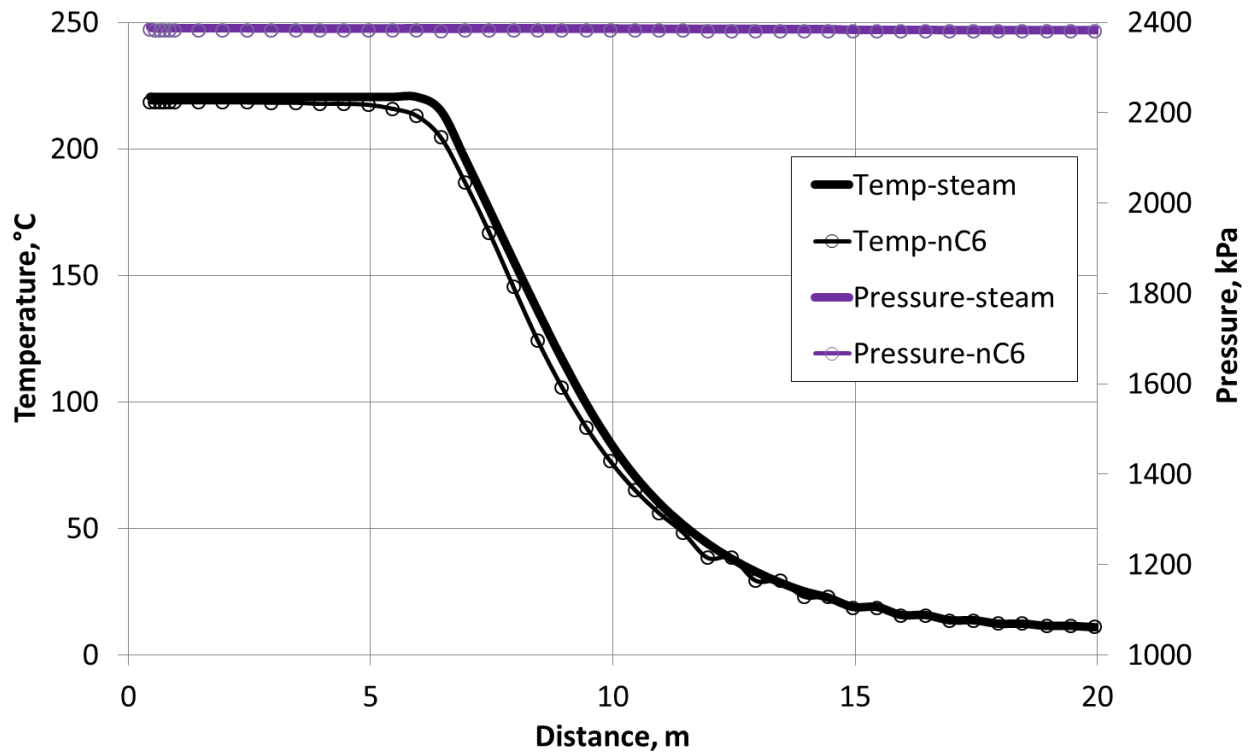


Figure 9. Horizontal temperature and pressure profiles for steam and steam-n-hexane co-injection cases after 1.5 year injection at $P_{inj}=25$ bar.

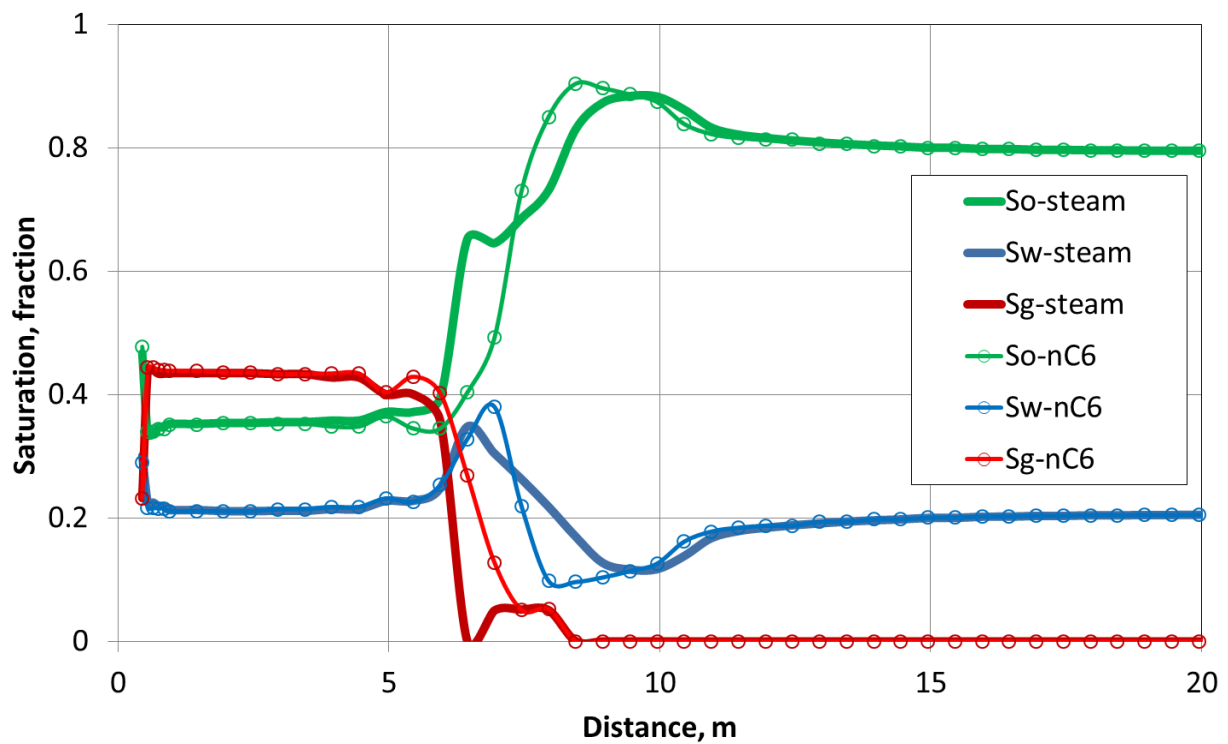


Figure 10. Horizontal saturation profiles for steam and steam-n-hexane co-injection cases after 1.5 year injection at $P_{inj}=25$ bar.

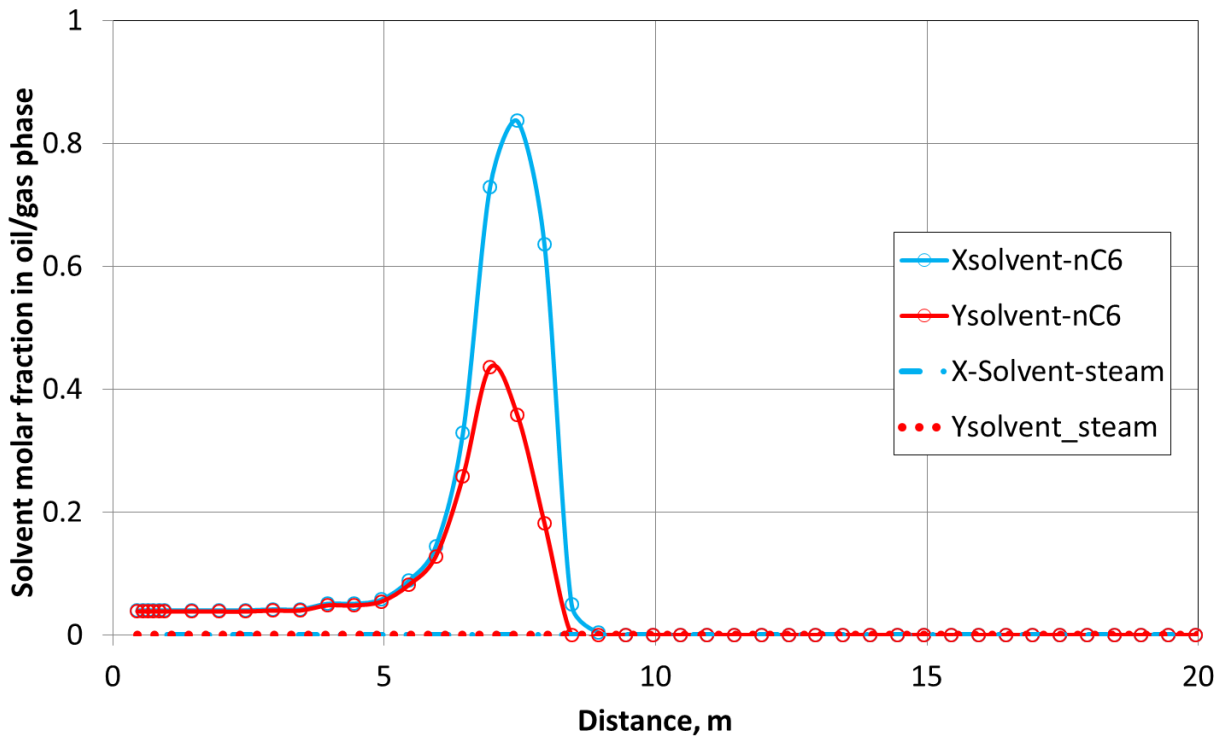


Figure 11. Horizontal solvent molar fraction in oil and gas phase for steam and steam-n-hexane co-injection cases after 1.5-year injection at $P_{inj}=25$ bar.

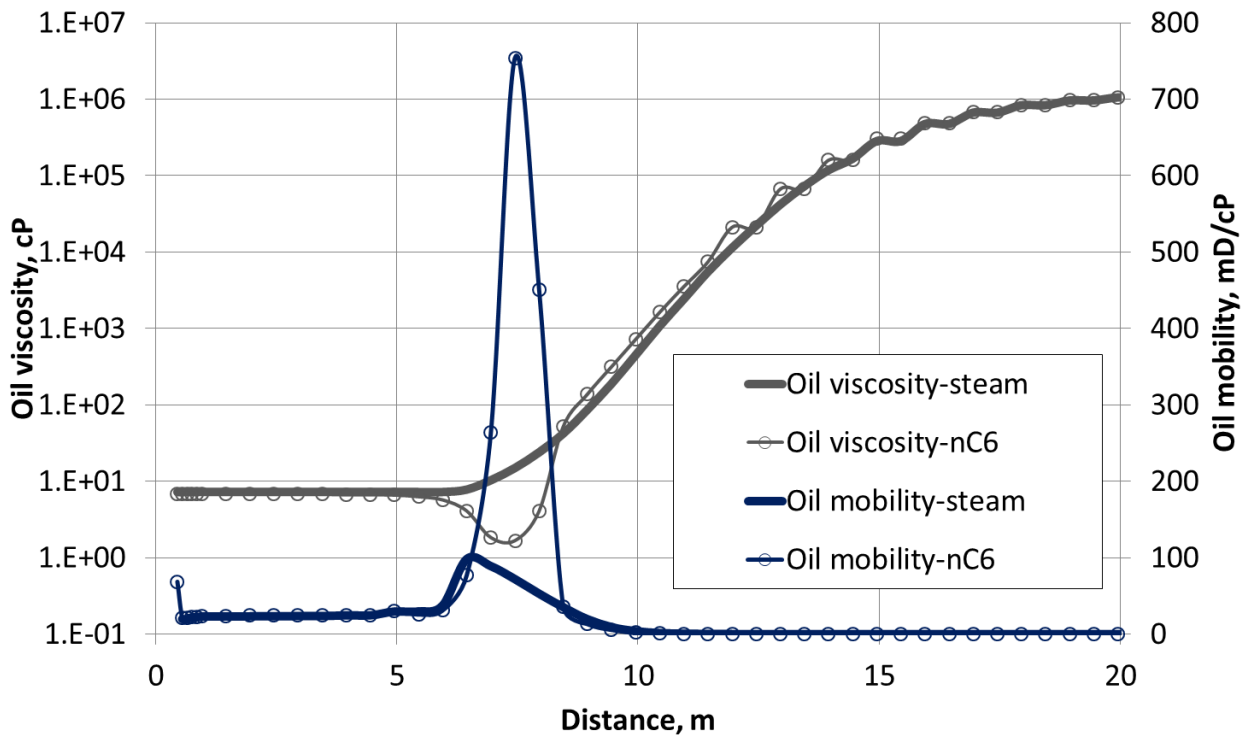


Figure 12. Oil viscosity and oil mobility for steam and steam-n-hexane co-injection cases after 1.5-year injection at $P_{inj}=25$ bar.

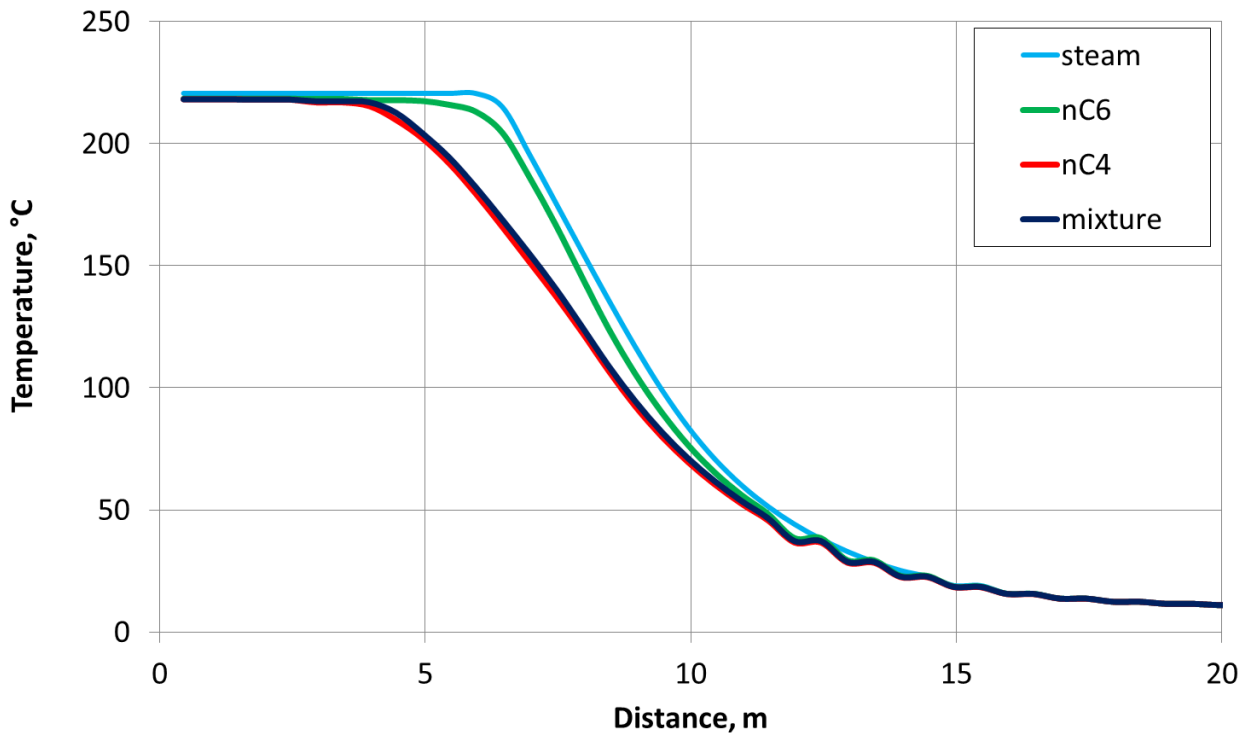


Figure 13. Horizontal temperature profiles for different solvents at $P_{inj}=25$ bar

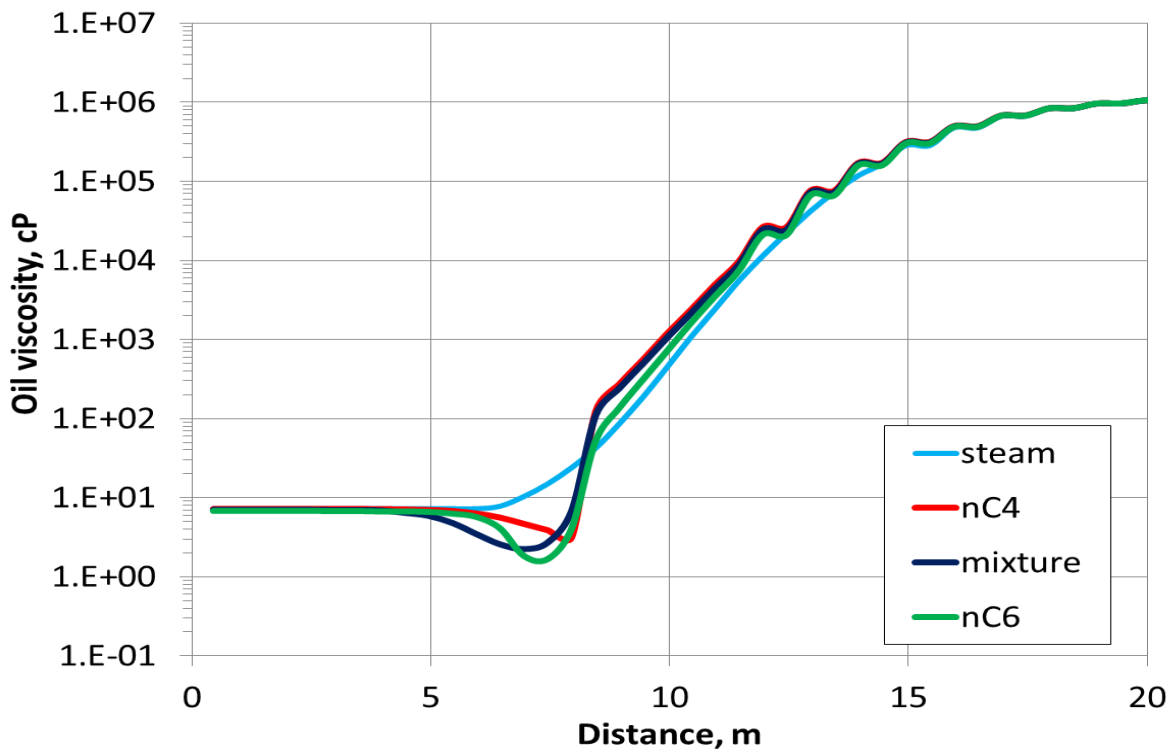


Figure 14. Oil viscosity profiles for different solvents at $P_{inj}=25$ bar.

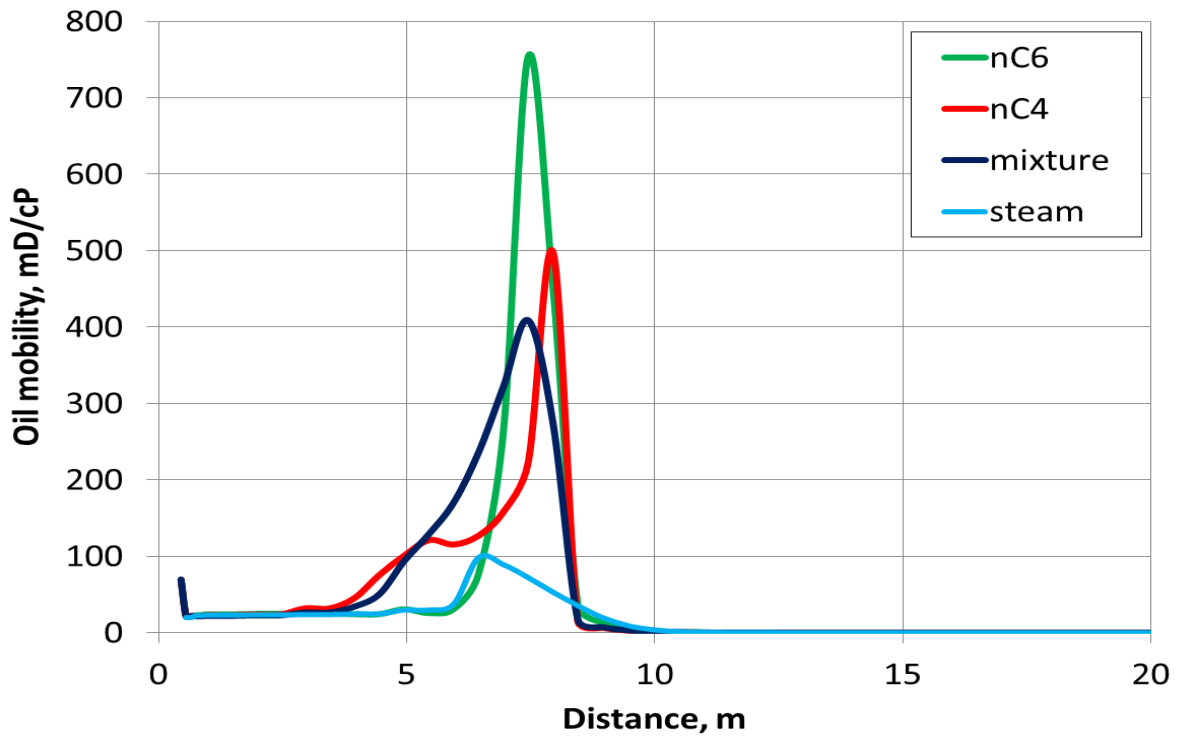


Figure 15. Oil mobility profiles for different solvents at $P_{inj}=25$ bar.

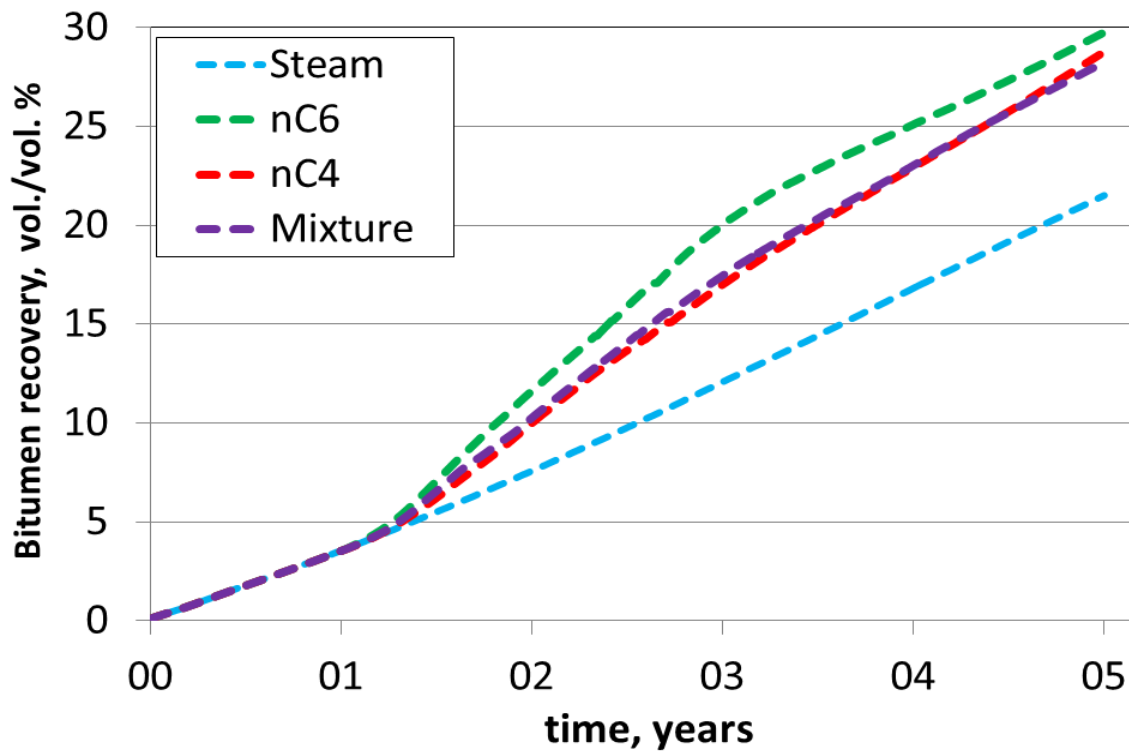


Figure 16. Bitumen recovery factor in volume percent (solvent no included) for different solvents at $P_{inj}=25$ bar.

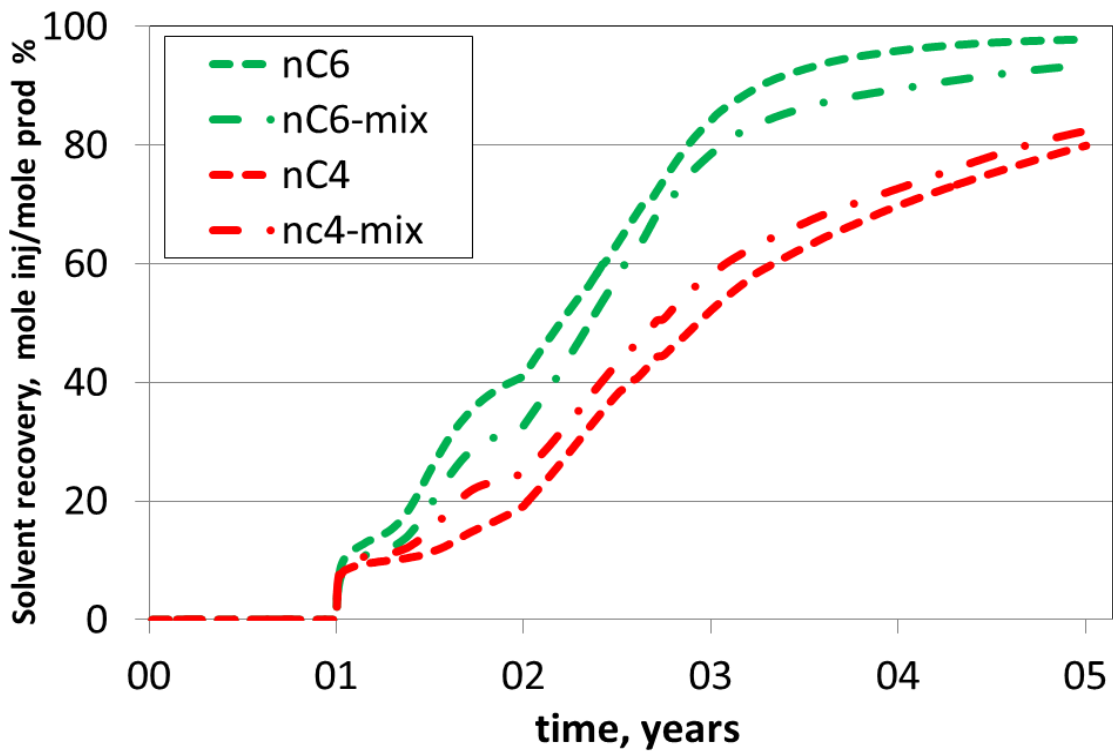


Figure 17. Solvent recovery in mole percent (produced/injected) for different solvents at $P_{inj}=25$ bar.

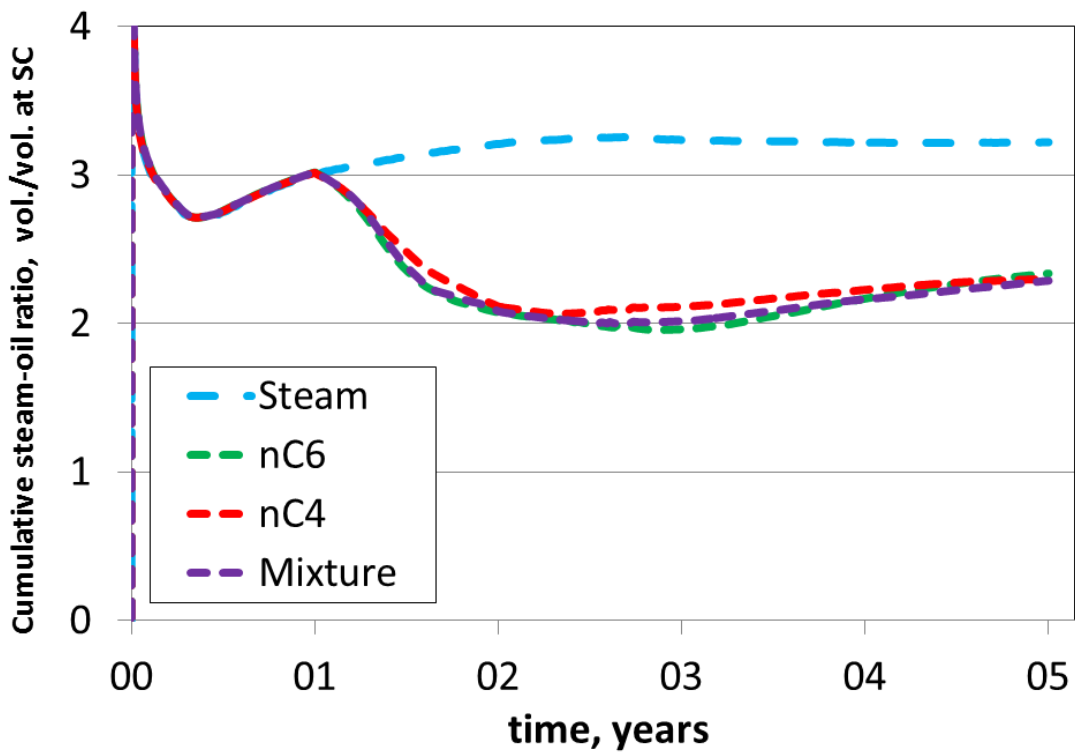


Figure 18. Cumulative steam-to-oil ratio for different solvents at $P_{inj}=25$ bar.

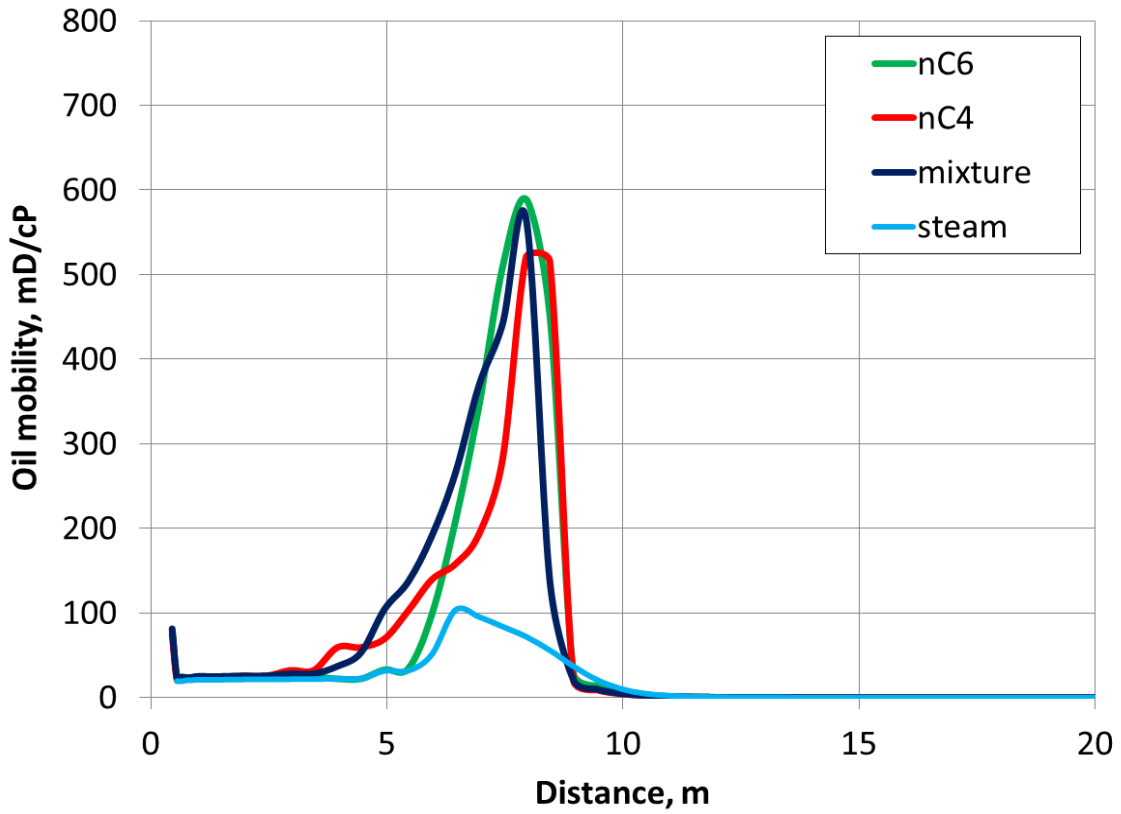


Figure 19. Oil mobility profiles for different solvents at $P_{inj}=35$ bar.

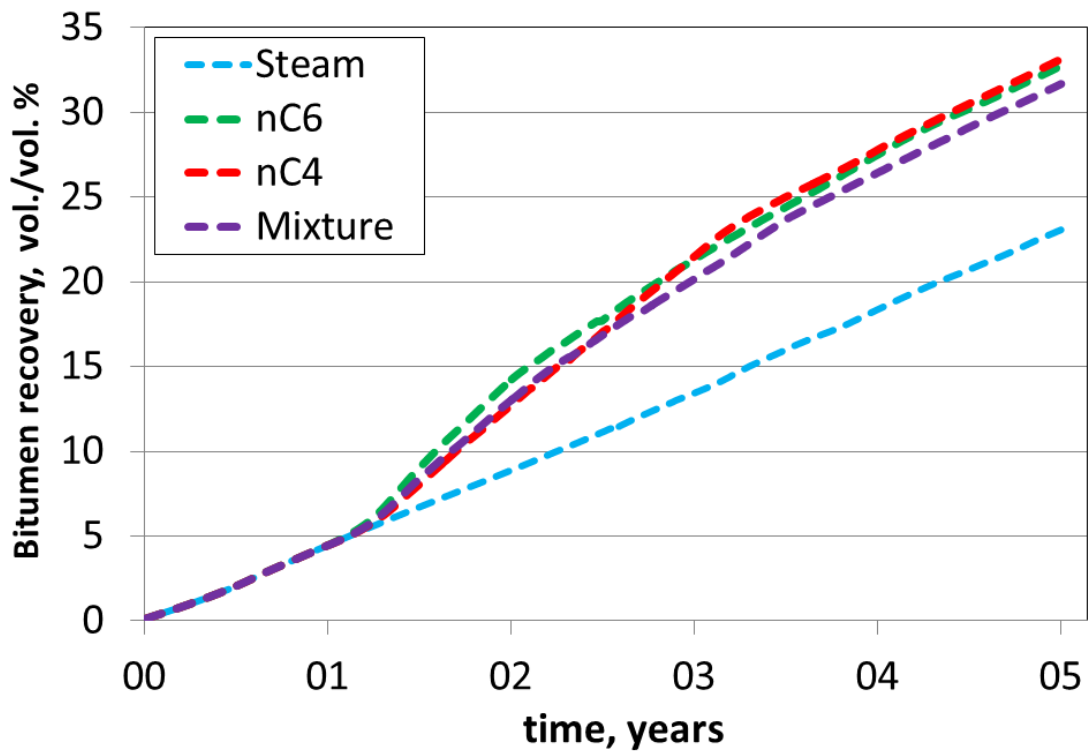


Figure 20. Bitumen recovery factor in volume percent (solvent no included) for different solvents at $P_{inj}=35$ bar.